Light attenuation experiments on double diffusive plumes and fountains

Bruce R. Sutherland,[1,2,a)] Brace Lee,[1] and Joseph K. Ansong[1]
[1]*Department of Physics, University of Alberta, Edmonton, Alberta T6G 2E1, Canada*
[2]*Department of Earth and Atmospheric Sciences, University of Alberta, Edmonton, Alberta T6G 2E3, Canada*

(Received 31 December 2011; accepted 7 June 2012; published online 29 June 2012)

By adapting the method of light attenuation to the study of axisymmetric disturbances, we examine the structure of forced plumes and fountains whose buoyancy is set by salinity and/or temperature differences between the turbulent flow and the otherwise stationary ambient. The attenuation measurements are used to infer the statistically steady-state density as a function of radius and height. These compare well with *in situ* measurements of density taken from a conductivity-temperature probe that repeatedly traversed the centreline of the plume. The theory for forced plumes also agrees well with the centreline density profile. The radial structure of plumes and fountains near the source is found to correspond well to a Gaussian profile, although the standard deviation is found to increase moderately faster with height than spreading rates reported in the existing literature. This is attributed in part to averaging biases resulting from light attenuating through transient eddies. In most experiments, hot and salty fountains reached a steady state height consistent with existing semi-empirical theories for fountains with just one diffusive component. However, if the density of the hot and salty fluid near the source is close to, but moderately larger than, that of the ambient, over time, the fountain is observed to increase progressively in height. This occurs presumably as a consequence of heat diffusion at the top of the fountain making the ambient above it increasingly buoyant relative to the negative buoyancy associated with less diffusive salt. [http://dx.doi.org/10.1063/1.4730431]

I. INTRODUCTION

Sour gas is a mixture of natural gas and hydrogen sulfide (H_2S), a highly toxic chemical.[1] Irritation to the eyes is noticed at 10 parts per million (ppm) and irritation to the lungs at 100 ppm. Respiratory paralysis and asphyxiation occur at 500 ppm, resulting in unconsciousness and death. The processing of sour gas separates hydrogen sulfide from the "sweet" natural gas. Hydrogen sulfide can be converted into elemental sulfur and hydrogen or otherwise burned in flares or incinerators. Flaring not only converts H_2S to sulfur dioxide and water, but it also heats the constituents, so decreasing the density of any unburned H_2S. The flare also creates a turbulent plume, which helps to dilute the concentration of H_2S in the plume by entraining air from in the surrounding ambient. If the efficiency of the flare is compromised and turbulence does not mix adequately then, because the density of H_2S is 18% greater than that of air at room temperature, the unburned H_2S gas may cool and accumulate at toxic concentrations at the ground. The process of understanding the complex problem of sour gas dispersion from flares has inspired several fundamental experimental-theoretical investigations including the study of fountains incident upon a model atmospheric inversion[2] and their evolution in a cross-flow.[3] Here, we take the ambient to be uniform and stationary in order to

a)E-mail: bruce.sutherland@ualberta.ca. URL: http://www.ualberta.ca/~bsuther.

focus upon the competing effects of positive buoyancy due to heat and negative buoyancy due to the large molecular mass of H_2S relative to air.

Observations, experiments, and the theory for plumes of buoyant fluid is well-established.[4–8] Also well-studied, though not so well understood, is the phenomenon of fountains in which dense fluid is injected upwards but ultimately falls back upon itself.[9–12] Both streams of investigation have assumed the density difference between the plume/fountain and ambient is established through temperature variations or through variations in concentration of a constituent, such as salinity. Not previously studied, however, is the phenomenon in which both temperature and constituent concentration vary in a plume/fountain at the source. In this work, experiments are performed to examine the structure and evolution of hot and saline plumes with the ultimate goal of understanding how hot but otherwise dense gas mixtures spread after emanating from a flare. Because the molecular diffusivities of heat and mass are typically different, we refer to plumes and fountains whose buoyancy are affected by both temperature and constituent-concentration differences as being "double diffusive." That said, the turbulent diffusivities of heat and salt do not differ significantly[13] and so one might not expect double diffusive effects to be manifest in a turbulent plume. However, turbulent processes are less prevalent at the top of a fountain and in the surrounding curtain of descending fluid. Double-diffusive effects may play a role in these regions.

A variety of experimental techniques have been used to examine the concentration field associated with plumes (for example, see Chen and Rodi[14] and List[8]). *In situ* thermocouple and hot-wire point measurements were taken by Shabbir and George.[15] Light sheet or laser-induced fluorescence (LIF) has been used non-intrusively to measure instantaneous cross-sections through a plume,[16] and this has been combined with particle-image velocimetry[17] to determine velocity as well as concentration fields.

One novel tool used in experimental analyses is the adaption of light attenuation methods to measure the concentration of disturbances. Using digital image analysis (e.g., see Dalziel[18]), it has been possible to measure the decrease in light intensity that attenuates when passing through dyed fluid or is scattered or absorbed by particles. In one class of applications, the change in light intensity was used to measure the depth of dyed fluid[19–21] and sediment deposits.[22] In a second class of applications, variations in light intensity gave a qualitative indication of across-tank mean concentration changes associated with mixing fluids.[23,24] Assuming the dye/particle concentration is approximately uniform across the line-of-sight spanning the tank and using calibration solutions to relate light intensity to concentration and/or density, it was possible non-intrusively to measure the mean across-tank concentration fields.[25–29]

Here, we have adapted this last method for application to axisymmetric, rather than spanwise-uniform disturbance fields. This novel method is an example of "absorption optical tomography."[30] Examples of axisymmetric disturbance fields include columnar vortices and laminar plumes or thermals rising from a localized source. The time-averaged structure of statistically steady turbulent jets and plumes emanating from localized sources are also axisymmetric, although the eddy field associated with them at a snapshot in time breaks this symmetry. The corresponding errors provide a useful test of the versatility of the axisymmetric inversion technique.

The theory of light attenuation for axisymmetric disturbances and tests of its application to an idealized circumstance is presented in Sec. II. Section III describes the experimental setup, digital imagery, and *in situ* probe measurement methods. These are applied in Sec. IV to the analysis first of a forced plume and then of a double diffusive fountain. The transitional case between plume and fountain is examined qualitatively. The implications of these results for understanding of pollutant dispersion from flaring are discussed in Sec. V.

II. AXISYMMETRIC LIGHT ATTENUATION

In the following, we review the well-established theory for light attenuation, we show how it can be adapted to predict the attenuation of light through an axisymmetric concentration field, and we explain how the problem can be inverted to get the concentration field from attenuated light intensity data. The results are then tested against an idealized example. Throughout, we orient the disturbance field so that light passes through it in the y direction and intensity is recorded as a function of x

and z. For axisymmetric disturbances, we assume rotational symmetry about the z-axis. Although we assume the disturbance field is independent of time, the inversion method can be applied to any particular snapshot of the intensity field to predict the concentration field, provided it is indeed axisymmetric.

A. Attenuation theory

When light passes through a dyed fluid its intensity, I, decreases with along-path distance y as

$$\frac{dI}{dy} = -\gamma C I, \tag{1}$$

in which C is the concentration of dye and the attenuation parameter, γ, depends on which dye is used (e.g., blue or yellow food colouring). More precisely, γ is a function of the wavelength of light being absorbed by the dye, but is independent of I, C, and y.

Assuming that C is uniform in the y direction, (1) can immediately be solved to give

$$I(y; x, z) = I_{00}(x, z) \exp(-\gamma C y), \tag{2}$$

in which I_{00} is the intensity of light incident upon the dyed region. Here, we have introduced the two spatial coordinates x and z lying in a plane perpendicular to the y-direction and it is understood that $C \equiv C(x, z)$ is independent of y.

From a calibration measurement in which the intensity I_s is recorded for light that has passed through a sample of width d having known uniform concentration C_s, one can explicitly determine the value of γ:

$$\gamma = -\frac{1}{dC_s} \ln\left[\frac{I_s}{I_{00}}\right]. \tag{3}$$

Ideally, this should be computed by recording the attenuation of monochromatic light. Measuring the attenuation of a white light source nonetheless gives a reasonably consistent measurement of a constant γ provided the transmitted fraction of the spectrum (e.g., blue light through blue dye) is small. This is the case in experiments reported upon here.

The assumption that γ is independent of I_s is valid provided the degree of attenuation is small[26,27] and the image is not over or under exposed. In an experiment for which the dye concentration is uniform across the width L_w of a tank, measuring the change in light intensity gives the concentration field at a snapshot in time

$$C(x, z) = -\frac{1}{\gamma} \ln\left[\frac{I(L_w; x, z)}{I_{00}}\right], \tag{4}$$

in which γ is found using (3).

Our intent here is to extend these ideas so as to determine the change in intensity for light passing through an axisymmetric concentration field. After modelling this forward problem, it is straightforward to solve the inverse problem in which the axisymmetric concentration field is determined from a measured intensity change.

The solution to the problem involves discretizing both the intensity and concentration fields in the x-y plane at an arbitrary level z, as illustrated in Figure 1. Here, light is assumed to propagate in the y-direction from the bottom to top of the schematic. It passes through concentric rings of width dr in which it is assumed the concentration within each annulus is uniform. We denote the concentration in the centre circle of radius $dr/2$ to be C_0 and the concentration in successive surrounding annuli to be C_1, C_2, etc. The intensity of light on the far side of the dyed disturbance varies in the x direction and is represented by discrete values $I_0 = I(0)$, $I_1 = I(dx)$, $I_2 = I(2\,dx)$, etc. Exploiting symmetry, I_0 is the intensity of light that has passed through the centre of the disturbance and I_1, I_2, etc., are the intensities recorded to the right of centre.

Assuming the incident light intensity I_{00} and the discrete concentration fields are known, we derive an approximate formula for the discrete intensities I_i, for $i = 0, 1, 2, \ldots$. The geometry is best set up to be neither over- nor under-determined if we take $dr = dx$ and assume the number

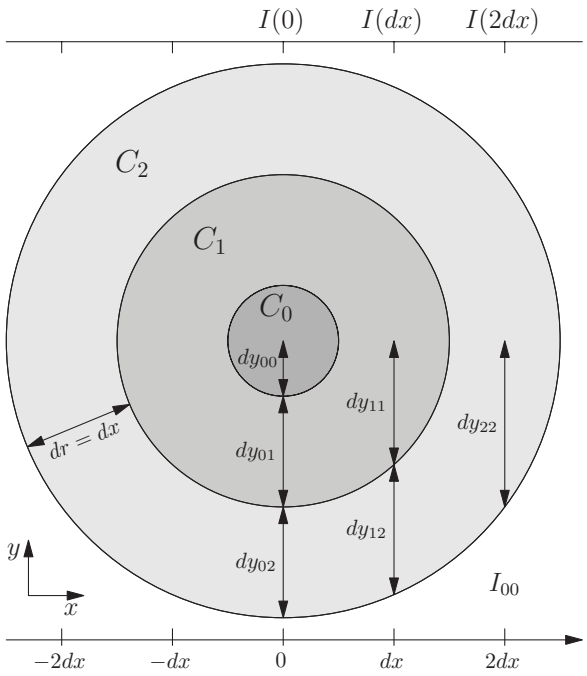

FIG. 1. Schematic showing the grid used to compute the forward problem of light attenuation by an axisymmetric distribution of dye as well as the inverse problem of determining the axisymmetric dye distribution from given light attenuation.

$N + 1$ of discrete concentrations C_j (for $j = 0 \ldots N$) equals the number of discrete intensities I_i (for $i = 0 \ldots N$). It is assumed that no attenuation occurs outside the outermost ring.

The trick to discretizing the problem in a way that becomes a simple matrix algebraic calculation is first to rewrite (1) as $d \ln(I)/dy = -\gamma C$ and then discretize the resulting integral to give

$$\ln(I_i/I_{00}) = 2\sum_{j=0}^{N}(-\gamma C_j)\, dy_{ij}. \tag{5}$$

The value dy_{ij} is the path-length for light originating from $x = i\,dx$, passing through ring j, and ultimately resulting in intensity I_i. These lengths are illustrated in Figure 1. Given the resolution $dr = dx$, the values of dy_{ij} are determined by a simple algorithm. In particular, $dy_{ij} = 0$ if $i > j$. Exploiting symmetry, we compute dy_{ij} over only the half of the concentration field facing the incident light. The attenuation over the other half has the same affect and so we multiply the sum in (1) by 2. If light originating from $i\,dx$ does not pass through ring j, we set $dy_{ij} = 0$.

The forward problem consists of specifying γ, discretizing $C(r)$ as $C_j = C(j\,dr)$, evaluating the sum in (5), and then exponentiating to determine the discretized intensity field $I_i = I(i\,dx)$. This can be done independently in successive horizontal planes ultimately giving a discretized representation of the two-dimensional intensity field $I(x, z)$.

Equation (5) can be represented explicitly as a matrix multiplication problem

$$\vec{\mathcal{I}} = -2\gamma\, \mathbf{DY}\, \vec{C}, \tag{6}$$

in which **DY** is a $(N + 1) \times (N + 1)$ square matrix with elements dy_{ij}, $\vec{C}$ is a vector with elements C_j, and $\vec{\mathcal{I}}$ has elements $\ln(I_i/I_{00})$. Thus, it is straightforward to solve the inverse problem in which the concentration field is determined from a given intensity field,

$$C_j = -\frac{1}{2\gamma}\sum_{i=0}^{N}\ln(I_i/I_{00})\, {dy_{ij}}^{-1}, \tag{7}$$

in which ${dy_{ij}}^{-1}$ are the elements of the inverse matrix $\mathbf{DY}^{-1}$.

B. Testing theory for axisymmetric plumes

As a first test of the method described above, we consider the theoretical prediction for the density field associated with a statistically steady, Boussinesq forced plume that rises in a uniform ambient. The equations for mass, vertical momentum, and buoyancy conservation are given respectively by[4,31]

$$\begin{aligned} \frac{dQ}{dz} &= \alpha\, 2\pi \bar{b}\, \bar{w} = 2\alpha\sqrt{\pi M}, \\ \frac{dM}{dz} &= -\pi \bar{b}^2\, \bar{g}' = -FQ/M, \\ \frac{dF}{dz} &= 0. \end{aligned} \tag{8}$$

Here, $Q = \pi \bar{b}^2\, \bar{w}$, $M = \pi \bar{b}^2\, \bar{w}^2$, and $F = \pi \bar{b}^2\, \bar{w}\, \bar{g}'$ are, respectively, the volume, momentum, and buoyancy fluxes for a top-hat plume, in which the vertical velocity $\bar{w}(z)$ and the reduced gravity $\bar{g}'(z)$ are assumed to be uniform over the width $\bar{b}(z)$ of the plume. The reduced gravity itself is defined in terms of the difference between the density of the plume $\bar{\rho}(z)$ and the density of the ambient ρ_a through $\bar{g}' = g(\bar{\rho} - \rho_a)/\rho_{00}$, in which ρ_{00} is the characteristic density. For a buoyant plume $\bar{g}' < 0$. Hence, the right-hand side of the momentum equation in (8) is positive, consistent with buoyancy acting to increase the upward momentum.

The entrainment parameter α, which measures the ratio of the horizontal inflow velocity to the vertical velocity, is assumed to be constant at each vertical level. Experiments give typical values of $\alpha \simeq 0.12$ for an ideal plume with a somewhat smaller value of $\alpha \simeq 0.08$ found for jet.[5,32] In the experiments reported upon below, we examine forced plumes as well as fountains (for which $\bar{g}' > 0$). As a compromise, we use the value $\alpha = 0.10$ as the entrainment coefficient for the theoretical calculations therein.

The equations describing the evolution with height of a Gaussian forced plume are again given by (8), from which solutions we set

$$\sigma = \bar{b}/2, \quad w_c = 2\bar{w}, \quad g'_c = 2\bar{g}'. \tag{9}$$

Here, $\sigma(z)$ is the standard deviation of the Gaussian, $w_c(z)$ is the maximum vertical velocity at the centre of the plume and $g'_c(z) = g(\rho_c - \rho_a)/\rho_{00}$ is the reduced gravity based upon the density difference between the centre of the plume and the ambient. With these definitions, $Q \equiv \iint w\, dA = 2\pi\sigma^2 w_c$, $M \equiv \iint w^2\, dA = \pi\sigma^2 {w_c}^2$, and $F \equiv \iint w g'_c\, dA = \pi\sigma^2 w_c g'_c$ are identical to the fluxes of the top-hat plume given below (8).

In testing the axisymmetric light attenuation method, we specifically consider a Gaussian plume with width $\sigma_0 = 0.1$ cm at the source where $z = 0$ and we suppose the maximum vertical velocity and relative density difference at the source are $w_{c0} = 1.0\,\text{cm/s}$ and $\Delta\rho_{c0}/\rho_{00} \equiv (\rho_{c0} - \rho_a)/\rho_{00} = -0.1$, respectively. The values have been chosen to be comparable to experimental parameters (see Sec. III A), but with numbers that make it easier to interpret the test results. The reduced gravity at the source g'_{c0} is found by multiplying the relative density difference by $g = 980\,\text{cm/s}^2$. The corresponding fluxes of volume, momentum, and buoyancy are $Q_0 = 2\pi\, w_{c0}\, {\sigma_0}^2$, $M_0 = \pi\, {w_{c0}}^2\, {\sigma_0}^2$, and $F_0 = \pi\, w_{c0}\, g'_{c0} {\sigma_0}^2$, respectively. These values are used to initialize the solution of (8). Integration proceeds by computing successive derivatives with a step-size of $\text{dz} = 7.8 \times 10^{-4}$ cm. Once $Q(z)$, $M(z)$ and $F(z) = F_0$ have been determined over a specified vertical distance, the equivalent top-hat width, vertical velocity, and reduced gravity at each height are found using

$$\bar{b} = \frac{Q}{\sqrt{\pi M}}, \quad \bar{w} = \frac{M}{Q}, \quad \bar{g}' = \frac{F}{Q}. \tag{10}$$

From these, we define the corresponding quantities for a Gaussian plume are defined using (9).

In particular, the relative density between the plume and ambient is

$$\frac{\Delta\rho}{\rho_{00}} = \frac{1}{g} g'_c(z) \exp\left(-\frac{r^2}{2[\sigma(z)]^2}\right). \tag{11}$$

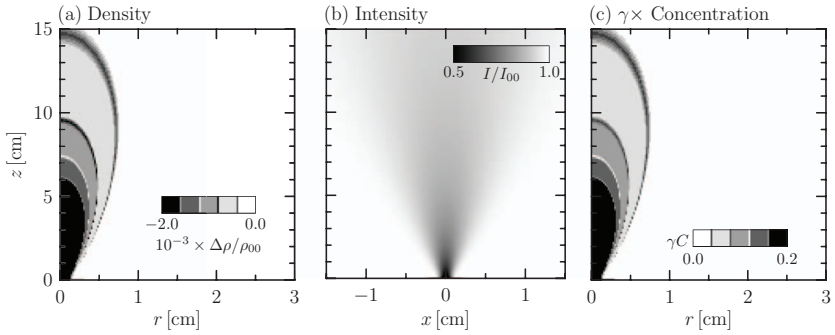

FIG. 2. Test of inversion method: (a) predicted density of a forced Gaussian plume with $\sigma_0 = 0.1$ cm, $w_{c0} = 1.0$ cm/s, $\Delta\rho_{c0}/\rho_{00} = -0.1$, and $\alpha = 0.1$; (b) the corresponding intensity of light passing through the plume computed by solving the forward problem (5) with dye attenuation coefficient $\gamma = 10$. (c) Result of solving the corresponding inverse problem, (7), to get γ times the concentration field.

This is shown in Figure 2(a). The calculation was performed on a domain of radius 3 cm and height 15 cm.

We now assume that light of incident intensity 1.0 passes through this plume. The concentration, c_0, of dye in the plume at the source is set to be unity. Treating this as a passive tracer, the concentration $\bar{C}(z)$ of dye satisfies

$$\frac{d}{dz}\left(\pi \bar{b}^2 \bar{w}\, \bar{C}\right) = 0. \tag{12}$$

Here, $\bar{C}$ is the concentration in a top-hat plume. The maximum concentration in a Gaussian plume is $C_c(z) = 2\bar{C}$. Rather than integrating (12), we may equivalently compute $\bar{C}$ using

$$\bar{C} = c_0 \frac{{b_0}^2 w_0}{\bar{b}^2 \bar{w}}, \tag{13}$$

in which b_0 and w_0 are the width and vertical velocity of a top-hat plume at the source. As expected, $\bar{C}$ satisfies

$$\bar{C} = c_0 \frac{\Delta\rho_c}{\Delta\rho_{c0}}. \tag{14}$$

So, the relative density of the plume can be determined directly from the concentration field.

Arbitrarily taking the attenuation parameter to be $\gamma = 10$, we solve the forward problem (5) at each vertical level to get the intensity field $I(x, z)$ recorded by a camera looking through this plume. The result is shown in Figure 2(b). In solving the forward problem, at each level z, the radial concentration field was discretized with a resolution of $dx = dr = 0.02$ cm. For convenience, we show the left- and right-side of the image about the centre of the model plume, although one is just the reflection of the other.

Finally, taking the intensity field to the right of the centreline as input, we use (7) to find the concentration field. This is plotted as the values γC in Figure 2(c). The figure shows that the relative density is indeed recovered after dividing the γC field by $\gamma = 10$ and multiplying by $(\Delta\rho_{c0}/\rho_{00})/c_0 = -0.1$.

C. Instantaneous and time-averaged attenuation

Forced plumes are only axisymmetric in a statistically time-averaged sense. At a snapshot in time, light is strongly attenuated through dye-containing eddies in the turbulent flow. Hence, averaging the intensity field to get an approximately symmetric image from which an axisymmetric concentration field is computed is not the same as averaging the concentration field. This is because as light passes through dye its intensity decreases exponentially, not linearly, with distance.

As a simple illustrative example, suppose a patch of dye of width d and concentration c crosses a light ray a fraction, f, of the time over which an image's intensity is averaged. The time-averaged concentration is $\langle c\rangle = fc$. However, using (1), the concentration determined from the average of the intensity field is

$$\bar{c} = -\frac{1}{\gamma d}\ln\left[fe^{-\gamma cd}\right] = c - \frac{1}{\gamma d}\ln(f).$$

If the motion is close to steady so that $0 \le \epsilon \equiv 1 - f \ll 1$, the error in the measurement is

$$\frac{\bar{c} - \langle c\rangle}{\langle c\rangle} \simeq \epsilon\left(\frac{1}{\gamma cd} - 1\right). \tag{15}$$

Light attenuation experiments are usually designed so that the light intensity does not change significantly when passing through the dye.[26,27] Hence, the product γcd is typically much smaller than unity. For this reason, we expect the error given by (15) to be small only if ϵ is sufficiently small compared with γcd.

III. EXPERIMENT SETUP AND ANALYSIS METHODS

A. Tank setup

The experimental setup is illustrated in Figure 3. A cubical tank measuring $L_T = 39.5$ cm on each side was filled to a depth $H_T = 38$ cm with either fresh or salt water of density ρ_a. This ambient density, measured with the Anton Paar DMA 4500 density meter, ranged in different

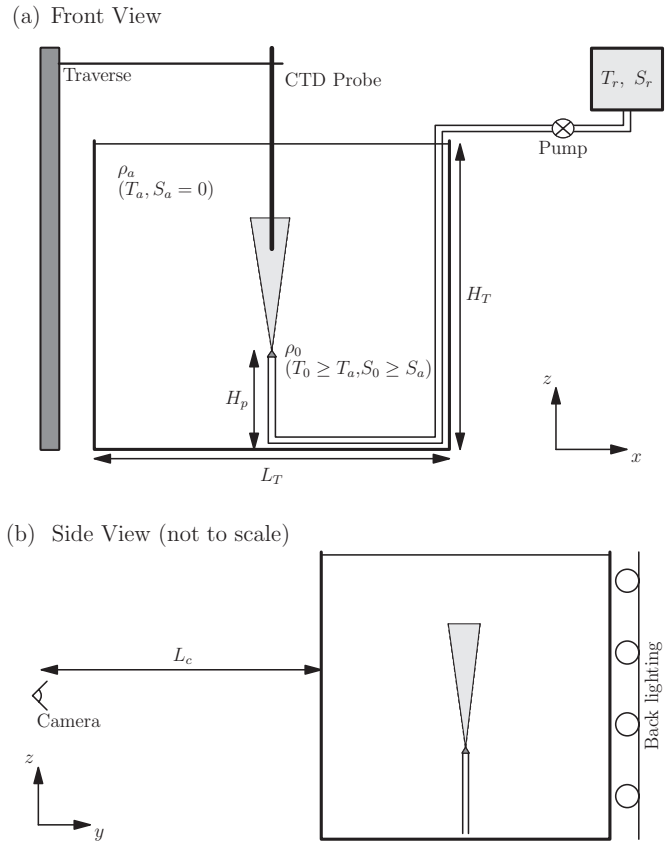

FIG. 3. Experimental setup showing (a) a front view of the tank, reservoir, and conductivity/temperature probe, and (b) a side view showing the camera and rear lighting.

experiments from $\rho_a = 0.998$ to $1.100\,\mathrm{g/cm^3}$. Separately, a reservoir was filled with 10 l of fresh or salty water, which ranged between boiling and room temperature. To this, we added 100–200 ml of blue food colouring. The fluid in the reservoir passed through a hose, with surrounding Styrofoam insulation, from the reservoir through a Monostat peristaltic pump, and then to a nozzle directed upward at the horizontal center of the tank. The tip of the nozzle, situated 16 cm above the bottom of the tank, had a radius of $b_0 = 0.2$ cm and was fitted with a mesh having 0.05 cm openings in order to trigger turbulent flow at the source. The flow rate was established by the motor-setting of the pump. In different experiments, this ranged from $Q_0 = 0.9$ to $1.7\,\mathrm{cm^3/s}$. The corresponding Reynolds number based upon the nozzle radius and vertical velocity was on the order of $Re \sim 200$.

Before the designated "start" of an experiment, the pump was turned on with a fixed motor speed. Although undyed fluid in the hose between the nozzle and reservoir was immediately observed to rise turbulently from the source, the experiment was deemed to have started (at time $t = 0$) when dyed fluid from the reservoir first emanated from the nozzle. This indicated that the saline and/or hot fluid from the reservoir had passed from the reservoir to the nozzle.

For typical experimental parameters, the system reached statistically steady state in 30 s (after $t = 0$). The radius of the disturbance to a height 15 cm above the source was less than 10 cm. This was sufficiently small that the tank side-walls did not influence the motion. The plume experiments stopped when the dyed fluid that accumulated near the top of the tank extended downward to within 15 cm above the nozzle; this typically was on the order of 10 min. Likewise, fountain experiments typically stopped after approximately 10 min when dense fluid pooling at the bottom of the tank accumulated close to the height of the nozzle. Over the duration of an experiment, the temperature of fluid in the reservoir decreased from 2°C to 4°C (about 10% to 20% of the temperature difference between the reservoir and ambient). In some fountain experiments, this change was evident as a gradual decrease in the steady state fountain height on the order of $1-3$ cm.

B. Camera measurements

In most experiments, a translucent sheet of white acrylic was placed behind the tank and this was illuminated from behind by a bank of fluorescent bulbs. On the opposite side, a distance L_c from the front of the tank, a digital camera was situated to look through the tank at the acrylic sheet with the centre of the field-of-view 8 cm above the tip of the nozzle and the zoom set to record an area 16 cm square at the vertical plane of the plume. The camera itself was situated between $L_c = 3.2$ and 4 m from the front of the tank. By positioning the camera so far from the tank while looking perpendicularly into a field of view with light entering the camera at a maximum angle of 1.5°, the effects of refractive index variations were minimized.

While the conductivity-temperature probe was situated near the surface of the ambient (see Sec. III C), successive snapshots of the plume were taken every second. An example of a single snapshot in Figure 4(a) shows dyed, fresh water injected into a salient ambient. The injected fluid was turbulent near the source, rapidly diluted, and spread through turbulent entrainment as it buoyantly rose far from the source. An ensemble of snapshots was averaged to give an image of the intensity associated with a statistically steady plume shown in Figure 4(b). Averaging had the effect of smoothing over localized regions of relatively high concentration, revealing an approximately axisymmetric disturbance. As is typical of a plume, this widened at a rate on the order of one tenth the height of rise.

In most experiments, the background intensity was approximately uniform having intensities of $I_{00} = 0.80 \pm 0.02$ in which 1 was white and 0 black. The attenuation parameter γ was found using (3) in which I_s was the intensity of light passing through the plume immediately above the source where $d = 0.4$ cm and $C_s \equiv c_0 = 1$. Typical values were found to range between $\gamma \simeq 1.0$ and $2.0\,\mathrm{cm^{-1}}$. The measured value was used in (7) to compute concentration and (for plume experiments) density fields from the intensity field measured by the digital camera.

Finally, the intensities at each point in the average image were divided by the corresponding background intensities determined from a snapshot of the experiment before it began. This is shown

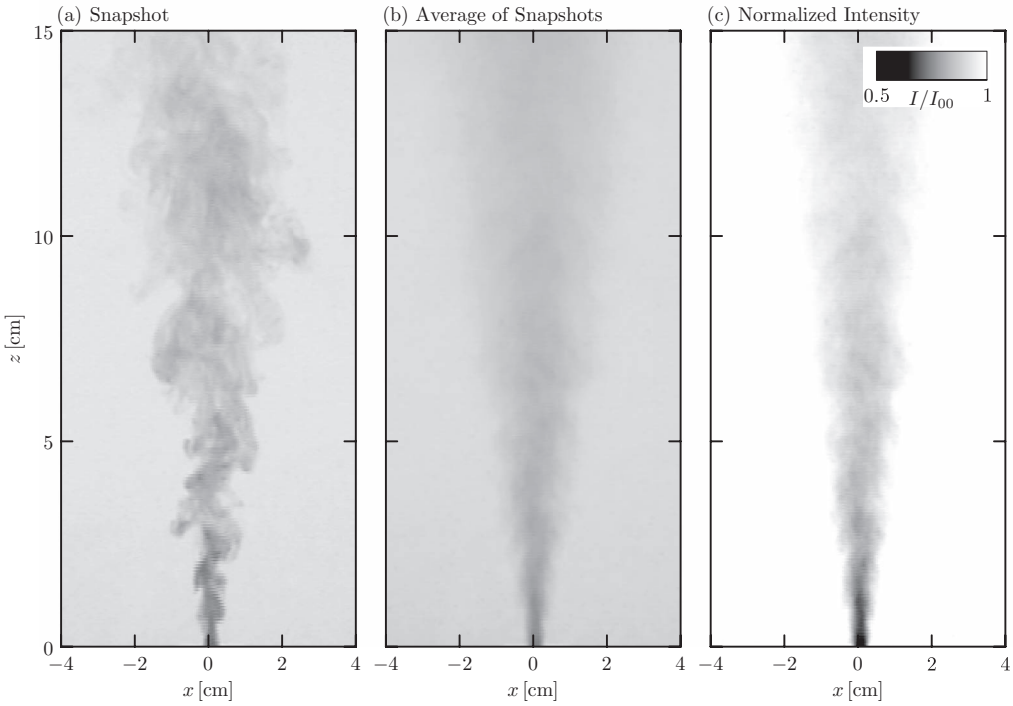

FIG. 4. (a) Snapshot from an experiment in which a forced plume of fresh water rises in a salt-water ambient. (b) Average of 21 such snapshots each taken 1 s apart. (c) Intensity of the average image normalized by the background light intensity determined before the start of an experiment. Experiment parameters are $b_0 = 0.2$ cm, $w_0 = 15.5$ cm/s, $\rho_0 - \rho_a = -0.0985$ g/cm^3.

in Figure 4(c). It is from this last field of computed relative intensities that we used the axisymmetric inversion code to compute concentrations and inferred their statistically steady state density as a function of r and z. In this non-idealized circumstance, the left- and right-hand sides of the intensity field were not necessarily identical. We separately inverted the right and left sides and also averaged the two together before inverting. This gave an estimate of the error associated with the resulting concentration field. If the plume axis was tilted due to poor source conditions or ambient circulations in the tank, the assumption of axisymmetry was broken and experiments were excluded from analysis.

In fountain experiments, it was useful to construct time series along a vertical line through the centre of the flow. As an example, Figure 5(a) shows a snapshot taken during a typical fountain experiment. The fluid in the fountain initially rose upward from the origin due to the momentum of the fluid at the source. But buoyancy acted opposite to the direction of the momentum so that the dense fluid ultimately collapsed back on itself. The collapsed fluid fell around the fluid rising from the source. Some of this downflow was entrained into the core of the fountain making the uprising fluid relatively more dense. And so, after some time, the fountain's height reduced from its initial maximum value to a lower steady-state height.

The fountain's evolution from its initially large overshoot to its final quasi-steady height is evident in the vertical time series shown in Figure 5(c). This image is constructed by extracting a column of pixels aligned above the center of the plume continuously over 600 s. The repeated downward and upward passage of the vertically traversing conductivity-temperature probe through the fountain's centre (see Sec. III C) is evident through the sequence of black spikes in this image. After the probe traversed back upward, there was a short recovery time before the fountain returned to steady state. Although salinity at the source was constant throughout the experiment, a decrease on the order of 1 cm of the "steady-state" height was observed over the duration of the time series due to a moderate temperature decrease of fluid in the reservoir.

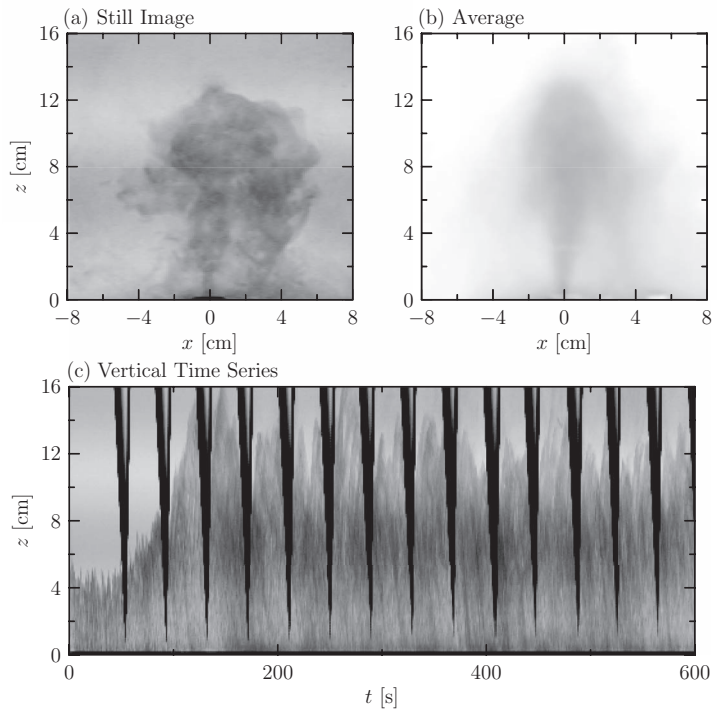

FIG. 5. Examination of a hot and saline fountain injected into a fresh ambient. Experimental parameters are $w_0 = 10.3\,\mathrm{cm/s}$, $T_0 - T_a = 12^\circ\mathrm{C}$, and $S_0 = 4.5$ ppt. Hence, the relative density of the fluid at the source is $\Delta\rho_0/\rho_{00} = 0.0008$. (a) Snapshot and (b) average of many snapshots with background removed. (c) Vertical time series through the centre of the fountain taken over 10 min from the start of the experiment at $t = 0$. The 14 black downward spikes in this image show the relatively slow descent and rapid ascent of the conductivity-temperature probe as it traverses repeatedly through the centre of the fountain.

C. Salinity and temperature measurement

The centreline composition of the plume was measured by a conductivity-temperature (CT)-probe, which combines a Fast Conductivity Sensor and a Thermometrics fast response FP07 thermistor (MicroScale Conductivity and Temperature Instrument, Precision Measurement Engineering).

Before the start of the experiment, the probe was calibrated using 12 samples of water with four different salinities of 0, 3, 6, and 10 ppt each with three different temperatures of 293, 303, and 315 K. Coefficients determined from these samples were then used to determine salinity and temperature from voltages recorded from the conductivity and thermistor sensors.

The probe was then attached to a traverse with the probe tip initially just below the surface of the water in the tank and positioned vertically above the plume nozzle.

After the start of an experiment once the plume or fountain reached a statistically steady state, the CT-probe traversed slowly downwards at 1 cm/s through the center of the plume/fountain to within 1 cm above the nozzle taking samples at 100 Hz. The probe then traversed rapidly upward without recording data and, after a pause of approximately 30 s, it traversed slowly downward again measuring the conductivity and temperature. The procedure was repeated up to 15 times or until the end of an experiment.

From the traverse data, successive vertical profiles of salinity and temperature were constructed and, from these, successive profiles of the centreline densities were computed. These were averaged to give an *in situ* estimate of $\rho_c(z)$ with the standard deviation giving a measure of the error associated with ρ_c.

An example of the temperature, salinity, and density profiles measured by the probe during a fountain experiment is shown in Figure 6. Profiles extracted from nine successive traverses are

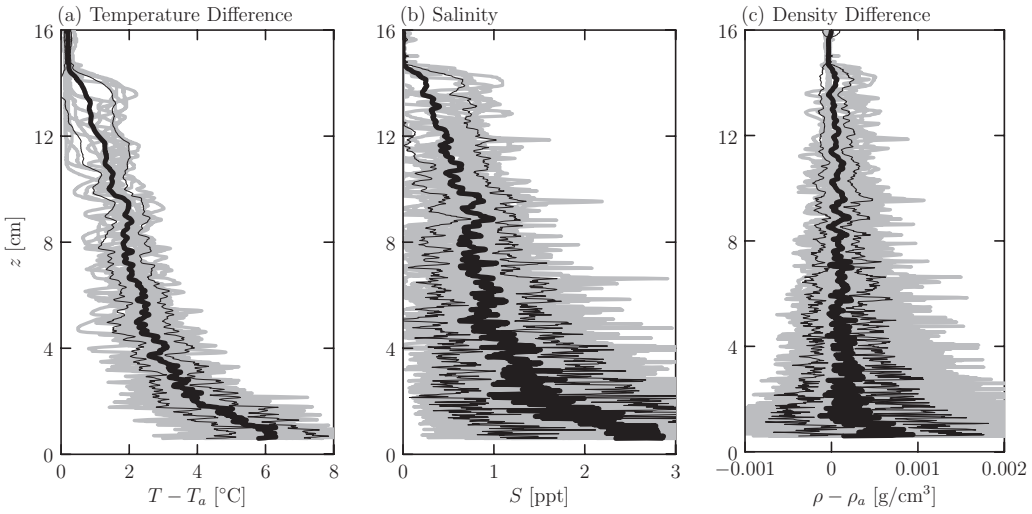

FIG. 6. (a) Temperature, (b) salinity, and (c) density ensembles from experiment whose parameters are given in Figure 5. Gray curves are data from individual probe measurements with the thick (thin) black curves representing their average (standard deviation about the average).

shown in gray with a thick black line indicating their average at each height. Averaging over the traverses reduces the amount of fluctuation due to the turbulent mixing in the fountain.

IV. RESULTS

Here, we first examine the density structure of a plume, using this as a test of the axisymmetric light attenuation method. The results are compared with CT-probe measurements and theory. Thereafter, we focus upon the structure of double-diffusive fountains in a fresh water ambient.

A. Plumes

As a test of the efficacy of the axisymmetric inversion method, we examined the structure of a forced buoyant plume of fresh water into a uniform but salty ambient of relative density $-\Delta\rho_0 = \rho_a - \rho_{00} = 0.0985$ g/cm^3. Both the plume and ambient had the same temperature. The plume was injected upwards through the turbulent nozzle of radius $b_0 = 0.2$ cm with volume flux $Q_0 = 0.974\,\text{cm}^3/\text{s}$. Hence, the mean injection speed was $w_0 = 15.5$ cm/s and the corresponding source momentum and buoyancy fluxes were $M_0 = 7.56\,\text{cm}^4/\text{s}^2$ and $F_0 = -94.1\,\text{cm}^4/\text{s}^3$, respectively. Snapshot and time-averaged images of the forced plume in this experiment are shown in Figure 4.

The predicted length scale for the transition from jet-like to plume-like behaviour is $H_\star \equiv (M_0{}^3/F_0{}^2)^{1/4} \simeq 0.5$ cm. So, the motion is expected to have transitioned to plume-like behaviour above $z \simeq 6H_\star \simeq 3$ cm, well within the experiment domain.

Figure 7 compares theoretical predictions with measurements of density using axisymmetric light-attenuation and with *in situ* conductivity probe data. The first two panels show the mean intensity and the value of γC found by axisymmetric inversion. In this experiment, we found $\gamma = 1.3\,\text{cm}^{-1}$. Rather than dividing by γ to get the concentration field, we additionally made the assumption that the concentration field was proportional to the density difference between the plume and ambient and so we also multiplied by the result by $\Delta\rho_0$ to get the relative density field $\Delta\rho \equiv \rho(r, z) - \rho_a$. This is shown in Figure 7(c).

The result is compared with the corresponding theoretically predicted density difference in Figure 7(d). The calculation was performed using an entrainment parameter of $\alpha = 0.1$. Comparing Figures 7(e)–7(g), we find that theory well-predicts the centreline density measured both by direct

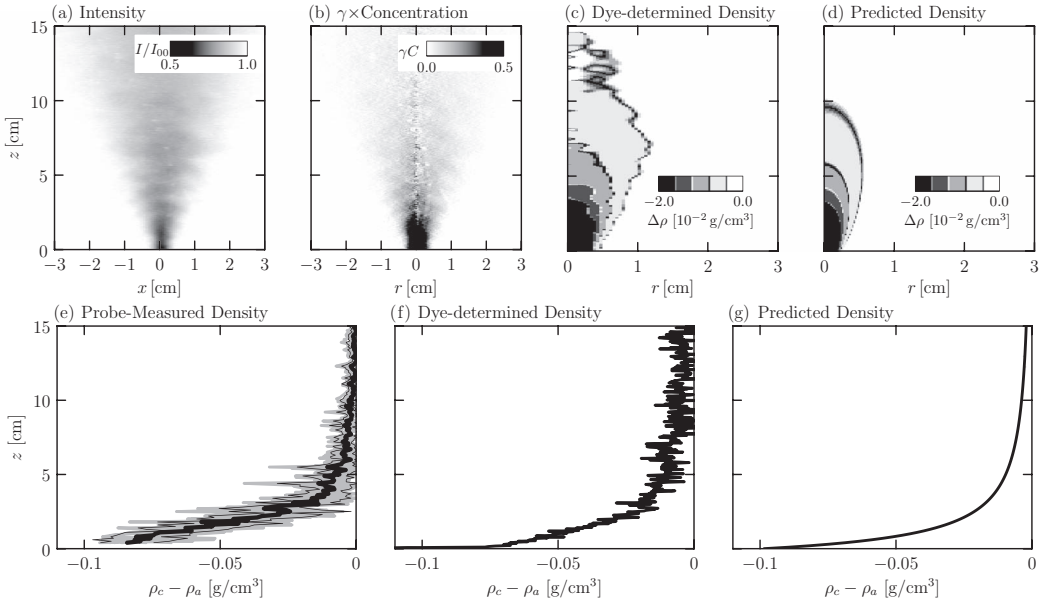

FIG. 7. Comparison of theory to a forced plume experiment whose parameters are the same as those given in Figure 4. (a) Average intensity (from Figures 4(c)), (b) the corresponding computed value of γC found by axisymmetric inversion, and (c) the corresponding density, which is compared with (d) the theoretically predicted density. (e) Centreline density profiles measured by the conductivity probe. Six successive profiles are taken 1 min apart (light gray lines). At each vertical level, these are averaged (thick black line) with errors given by the standard deviation (thin black lines). Centreline density determined by (f) light-attenuation and (g) theory.

conductivity probe measurements and by light-attenuation. All show a rapid increase with the height of the plume density asymptotically approaching that of the ambient.

In experiments (not shown) of forced warm and salty plumes in which the fluid at the source was buoyant ($\Delta\rho_0 = \Delta\rho_{T0} + \Delta\rho_{S0} < 0$), we likewise observed a rising plume whose centreline density measured directly by the CT-probe and indirectly by light attenuation matched well with theory. This may be anticipated because entrainment and mixing in plumes are turbulent processes. Although the molecular diffusivity of heat is 70 times that of salt, their turbulent diffusivities and consequently their entrainment rates are about the same.[13]

Simply by looking at images of time-averaged intensities, one can estimate the spreading rate of a plume. For example, in Figure 7(a), one can track the albeit fuzzy boundary between the dyed fluid associated with the plume and the clear ambient. From this, one can estimate the radial spreading rate with height to be 0.13 ± 0.02, consistent with the predicted spreading rate of an ideal top-hat plume for which $db/dz = (6/5)\alpha \simeq 0.12$, for an entrainment parameter of $\alpha = 0.10$.

Using the results of axisymmetric light-attenuation, we can attempt to make a more accurate quantitative measurement of the spreading rate of the plume. Figure 8 shows the radial structure of the relative density of the plume at discrete heights as determined by light-attenuation. The thick gray lines plot radial profiles of relative density at successive vertical heights, which are extracted from successive radial cross sections through the data shown in Figure 7(c). From these profiles, we determined the amplitude and standard deviation of the best-fit Gaussian functions to these plots, as described in Appendix A. These computed curves are superimposed as thin black lines on the profiles taken at $z = 1, 2, \ldots 6$ cm. The thick solid line in Figure 8 shows the best-fit standard deviation between $z = 1$ and 6 cm. The best-fit slope of this line between $z = 2$ and 6 cm shows that the standard deviation increases with height as $\beta_\sigma \equiv d\sigma/dz = 0.09\,(\pm 0.01)$, consistent with the measured[16,33] spread of concentration in a plume as $\beta_\sigma \simeq 0.08$ (though originally given in terms of the "1/e-width" spreading rate of 0.112). Because the equivalent top-hat radius is $b = 2\sigma$ the corresponding increase of the top-hat width is $\beta \equiv db/dz = 0.18\,(\pm 0.02)$. The top-hat spreading rate for plumes cast in terms of the entrainment parameter α is $\beta = (6/5)\alpha$. Thus, we have indirectly

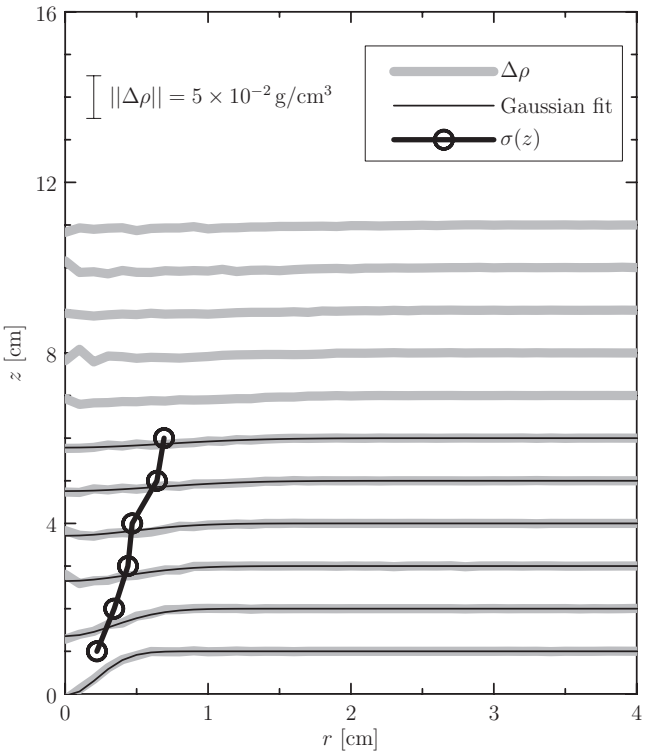

FIG. 8. Vertically offset radial profiles of density (thick gray lines) extracted from the light-attenuation data shown in Figure 7(c). Profiles are plotted every 1 cm from bottom to top at $z = 1$ cm, ... $z = 11$ cm above the source. Best-fit Gaussian curves are superimposed as thin black lines on the curves between $z = 1$ and 6 cm. The circles connected by a thick black line shows values of the standard deviation $\sigma(z)$ computed from radial profiles between $z = 1$ and 6 cm.

measured the entrainment coefficient to be $\alpha \simeq 0.15\,(\pm 0.02)$. This value is approximately 50% larger than the entrainment parameter determined from a range of plume experiments.[34] In part, this discrepancy may be because the width of a plume determined by vertical velocity variations through laser-Doppler velocimetry is approximately 20% smaller than the concentration width measured through laser-induced fluorescence.[16]

The discrepancy may also be attributed in part to biases with the experimental technique. As described in Sec. II C, we expect the light attenuation method over-predicts the actual statistically steady-state width of the forced plume in our experiments. This is because the image-average computed from a sequence of snapshots is not the same as the image conceptually produced from light passing through the time-averaged and axisymmetric field. Transient eddies near the radial extremes of the plume bias the image-average making it appear wider than the extent of the time-averaged concentration.

Imagining the eddies as transient patches of dyed fluid, the signal error is crudely estimated by (15), in which d represents the patch size and ϵ is the fraction of time light does not pass through this patch. In actual plume experiments, the corresponding values of ϵ and d are hard to estimate. Nonetheless, looking at the snapshot image of a plume in Figure 4(a), it is clear that the flow is more transient (ϵ is larger) near the radial extremes of the plume than at its center. For this reason, light attenuation is prone to over-predict the radial extent of concentration field.

Through this reasoning, all the quantitative results of light-attenuation might be put into question. However, we have shown that the centreline prediction is accurate. Furthermore, the process of axisymmetric inversion from intensity to concentration field using (7) puts more weight on data gathered from light passing through the plume centreline. And so fitting a Gaussian to the concentration field near $r = 0$ does nonetheless produce a reasonable measure of the radial spreading of the plume close to the source where the plume radius is not so wide.

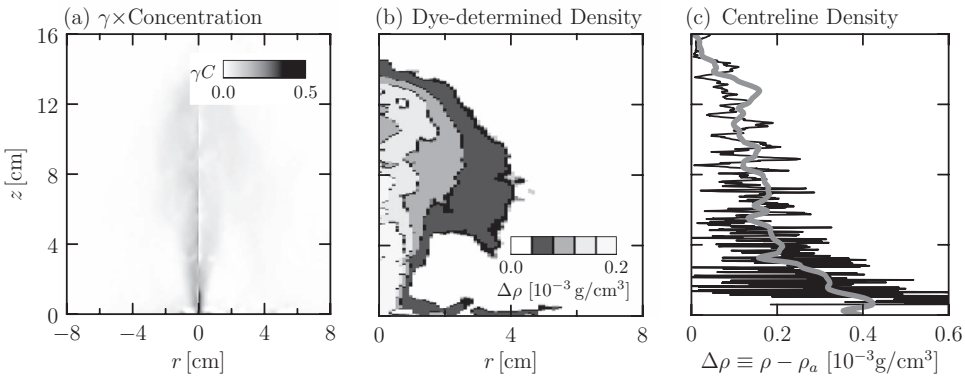

FIG. 9. (a) Concentration as a function of radius and height for a fountain, as illustrated in Figure 5. The fields computed separately from the right-hand and left-hand sides of the image-average are shown respectively to the right and left in (a). (b) The corresponding density difference computed from the average of the right-hand and left-hand concentration fields. (c) The corresponding centreline density found form axisymmetric dye attenuation (gray line) compared with the average of probe measurement (black line), reproduced from the thick black line in Figure 6(c).

B. Fountains

In experiments for which the total density due to temperature and salinity was sufficiently larger than the ambient density, the upward-injected fluid ultimately collapsed upon itself as a fountain. The theory for fountains is not so well established as that for forced plumes in part due to the influence of the opposing momentum of the collapsing fluid and also due to the entrainment of this fluid into the upward flow.[10,12] Nonetheless, we were able to measure the centreline density and to use light attenuation to gain insight into the spatial distribution of density in the fountain.

Figure 9 shows the results of using the light attenuation and probe measurements to determine the density of the fountain experiment shown in Figure 5. The experimental parameters were $Q_0 = 1.28\,\text{cm}^3/\text{s}$ (hence, $w_0 = 10.3\,\text{cm/s}$), $S_0 = 4.5$ ppt, and $T_0 - T_a = 12°\text{C}$. Hence, the relative densities due separately to salinity and temperature were $\Delta\rho_{S0} = 0.0033\,\text{g/cm}^3$ and $\Delta\rho_{T0} = -0.0025\,\text{g/cm}^3$, respectively. The combined relative density at the source, $\Delta\rho_0 = \Delta\rho_{S0} + \Delta\rho_{T0} = 0.0008\,\text{g/cm}^3$, was used to compute the corresponding momentum and buoyancy fluxes, $M_0 = 13.2\,\text{cm}^4/\text{s}^2$ and $F_0 = 1.02\,\text{cm}^4/\text{s}^3$, respectively.

Despite some asymmetry between the light-attenuation on the left- and right-hand side of the images, the separate axisymmetric inversions of each side of the normalized intensity image in Figure 5(b) gave the comparable values of $\gamma C(r, z)$ to the left and right of the centreline (see Figure 9(a)). Averaging the two sides and converting from γC to relative density by multiplying by 0.002 gave the density field, shown in Figure 9(b). Like a jet or plume, the centreline density decreased rapidly with height above the source. However, the fountain clearly showed the increase of relative density with radial distance far from the centreline associated with the descent of dense fluid around the central core. Measurements of centreline density from the CT-probe were consistent with those determined non-intrusively from light-attenuation, as shown in Figure 9(c).

As in Figure 8, successive radial profiles of density were extracted from the field shown in Figure 9(b) and Gaussian curves were fit to data near the centreline for profiles taken at $z = 1$, $2, \ldots$ 5 cm above the source. These are plotted in Figure 10. At heights not far above the source the fluid near the core of the upward jet expanded as a widening Gaussian virtually unaffected by the surrounding dense descending fluid. Above $z = 8$ cm the wider central Gaussian associated with the upflow is more difficult to distinguish from the descending flow around it.

The best-fit line through the origin for $\sigma(z)$ values between $z = 2$ and 6 cm has a slope of $\beta_\sigma = 0.21 \pm 0.014$, indicating a spreading rate more than twice larger that found in the forced-plume experiment (Figure 8). Using $\bar{b} = 2\sigma$, the corresponding spreading rate for a top-hat fountain is $\beta \simeq 0.42$. An increased spreading rate for a fountain relative to that for a plume is consistent with the predicted[4] top-hat spreading of a jet as $\beta = 2\alpha$, and it is consistent with the flattening

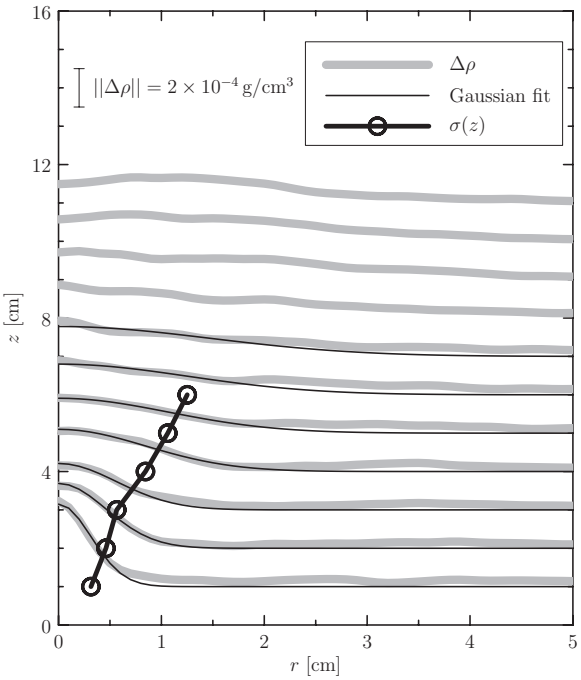

FIG. 10. Vertically offset radial profiles of density (thick gray lines) extracted from the plot shown in Figure 9(b) and shown from bottom to top at $z = 1$ cm, ... $z = 11$ cm above the source. Best-fit Gaussian curves near $r = 0$ are superimposed as thin black lines. The circles connected by a thick black line show values of the Gaussian standard deviation $\sigma(z)$ computed between $z = 1$ and 6 cm.

expected by the opposing momentum as well as with the entrainment of the relatively dense fluid associated with the downflow. However, our measured value is twice that determined by Baines and Chu[35] ($\beta = 0.17$) and Ansong, Anderson-Frey, and Sutherland[3] ($\beta \simeq 0.23$). The latter value was determined indirectly through measurement of the maximum height of a fountain in a moderate cross-flow. Although, light attenuation gives a direct measurement of the spreading rate, its value may exhibit measurement biases as a consequence of over-estimating concentrations radially far from the centreline, as discussed in Sec. IV A.

Because buoyancy opposes the initial direction of momentum in a fountain, the length scale

$$H_\star \equiv ({M_0}^3/{F_0}^2)^{1/4} \tag{16}$$

provides a characteristic measure of the fountain height. Explicitly, the experiments of Turner[9] predict the initial maximum height of the fountain should be $H_0 \simeq 2.1 H_\star$ and, after the fountain falls back upon itself, the steady-state maximum height should be

$$H = 0.7 H_0 \simeq 1.5 H_\star. \tag{17}$$

From the parameters for the experiment shown in Figure 9, we computed the characteristic height to be $H_\star \simeq 6.9$ cm. The corresponding vertical time series in Figure 5(c) shows that the observed steady-state maximum height vacillates around $12(\pm 2)$ cm $\simeq 1.7(\pm 0.3) H_\star$, moderately larger than the empirical prediction of Turner[9] but consistent within fluctuation errors. (See also the corresponding probe and attenuation measurements in Figures 6(c) and 9(c), respectively.) The maximum initial excursion apparent in the time series is approximately $15(\pm 1)$ cm $\simeq 2.2(\pm 0.1) H_\star$, consistent with the empirical prediction.

Similarly examining vertical time series extracted from movies of a wide range of double diffusive fountain experiments, we measured the steady-state maximum height. Comparing these results with theory in Figure 11, we generally found good agreement within errors.

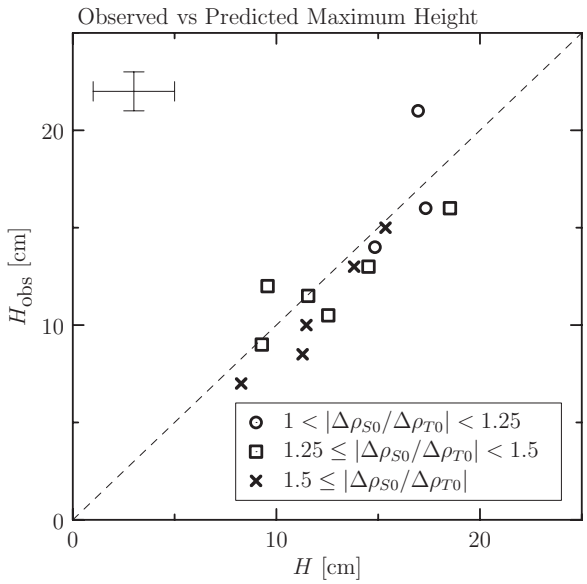

FIG. 11. Observed maximum height of fountain, $H_{\rm obs}$, plotted against the theoretically predicted maximum height, H. The dashed line indicates where theory matches observations. Typical error bars are indicated in the upper left-hand corner.

The analyses of the plume and fountain experiments suggest that their dynamics depend only upon the total relative density, $\Delta\rho = \Delta\rho_S + \Delta\rho_T$, resulting from the composition of density due to salinity and temperature. Although the molecular diffusivity of heat is almost two orders of magnitude greater than salt, the turbulent processes rendered their effective diffusivities to be almost equal, consistent with the mixing box experiments of Turner[13]

Nonetheless, we observed some evidence of double diffusive behaviour in experiments for which the temperature and salinity anomalies at the source resulted in nearly zero but positive buoyancy flux (i.e., $\Delta\rho_{T0} \gtrsim -\Delta\rho_{S0}$) and for which the source momentum flux was sufficiently small that $H_0 = 2.1H_\star$ was situated below the tank surface. In such circumstances, the greater molecular diffusion of heat influenced the less turbulent dynamics near the top of the fountain, significantly changing its long-time evolution. This is discussed next.

C. Fountain-to-plume transition

Figure 12 shows snapshots and vertical time series from an experiment exhibiting characteristics of both fountains and plumes. In this experiment, $\Delta\rho_{S0} \simeq 0.0041$ g/cm^3 and $\Delta\rho_{T0} \simeq -0.0038$ g/cm^3. The total source momentum and buoyancy fluxes were $M_0 \simeq 12\,\text{cm}^4/\text{s}^2$ and $F_0 \simeq 0.3\,\text{cm}^4/\text{s}^3$, respectively. So, $H_\star \simeq 11$ cm and $H = 17$ cm. The snapshots show that the flow initially behaved as a fountain, peaking about 12 cm above the source approximately 30 s after injection and then slumped to a lower peak height after 60 s. The peak then rose steadily reaching the surface at $z = 28$ cm after 100 s. Although much of the dyed fluid originating from the source spread across the surface, some also descended around the central jet. Thus, the flow exhibited both the buoyant behaviour expected of a plume as well as the negatively buoyant behaviour expected of a fountain.

To understand this, we consider the relative diffusion of heat and salt at the top of a fountain. In Appendix B, we estimate the length scale, δ_κ, over which heat and salt molecularly diffuse over the time a fluid parcel is situated near the top of a fountain. As given by (B3), the diffusion scale relative to the height of the fountain top is proportional to $\kappa^{1/2}M_0^{-1/4}$, in which κ is the diffusivity.

Near room temperature the diffusivity of heat is 70 times greater than that of salt in water. Hence, we might expect warm water to blanket the fountain top over a shell approximately eight times thicker than the corresponding shell of diffused salt. If sufficiently thick, compared with the

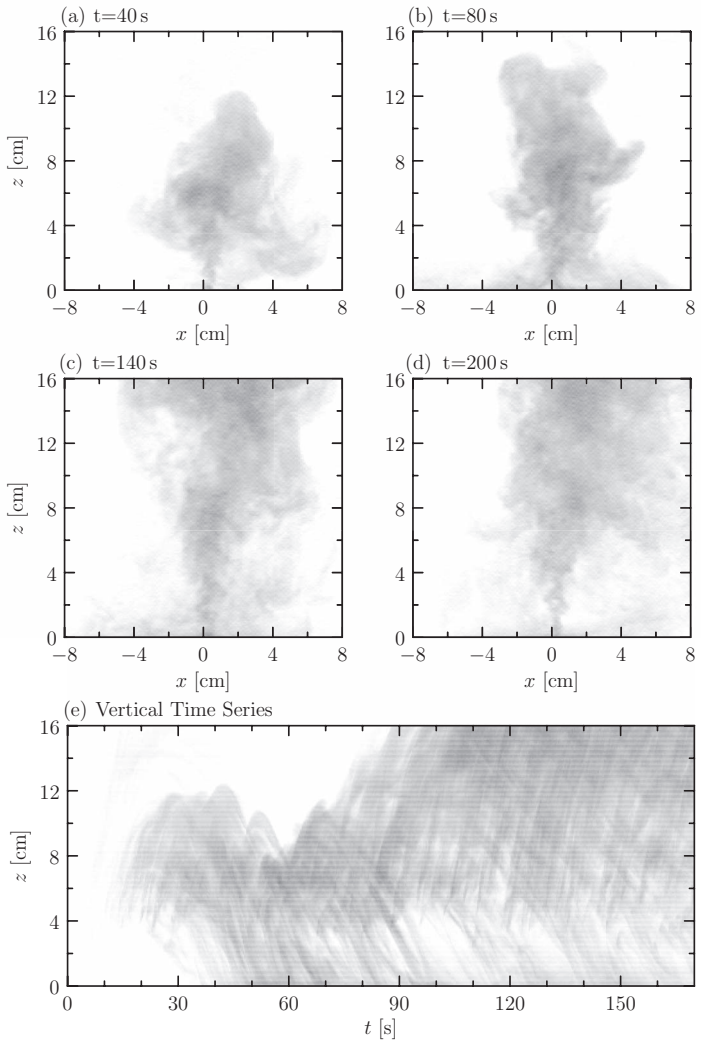

FIG. 12. Snapshots taken at the indicated times and vertical time series showing a double diffusive fountain exhibiting both plume and fountain behaviour. Here, $\Delta T_0 = 18^\circ$C, $\Delta S_0 = 5.5$ ppt, and $Q_0 = 1.24$ cm^3/s. The time series is constructed from a vertical slice taken 1 cm to the right of the centre of the source and to the right of the vertically traversing conductivity probe.

fluctuations at the top of the fountain, this warmed layer could precondition the ambient above the fountain allowing it to rise gradually over time.

For the experiment shown in Figure 12, for which $M_0 \simeq 12\,\text{cm}^4/\text{s}^2$, we compute the thickness of the diffusively heated shell to be $\delta_\kappa \simeq 0.02R_0$, in which $R_0 \equiv \beta H_0$ is the approximate radius of the fountain near its maximum height (see Appendix B). This value is not so large to warm the ambient substantially above the fountain top in the time a fluid parcel is situated in its cap. However, the warming could be enhanced by transient turbulent ejections of fluid from the fountain top. And over time such warming could be sufficient to render the ambient above the fountain top to be sufficiently buoyant to rise as a plume, carrying some of the dyed and saline fluid with it. Hence, the appearance of both plume and fountain-like behaviour in Figure 12.

These dynamics are qualitatively similar to those of the diffusive convection-mode of double-diffusive systems.[36–38] In many such studies, the vertical advance of the top of the convective layer is small because the ambient is stratified and also because the density difference across the interface between the ambient and convecting fluid is large so that motions at the interface are close to laminar. In the experiment shown in Figure 12, the density of the fountain is close to that of the (uniform)

ambient. And so the interface between the fountain top and ambient is continually disrupted by turbulent fluid parcels that penetrate into the ambient. This allows the fountain top to rise more rapidly upward into the ambient.

V. DISCUSSION AND CONCLUSIONS

We have described a matrix inversion algorithm by which light attenuation through an axisymmetric source can be used as a non-intrusive measure of the concentration field associated with the source itself. Though not as accurate as LIF[16,17] when applied to turbulent plumes, it is relatively simple and inexpensive to set up while still providing useful data. The method has been shown to work in principle for truly axisymmetric disturbances. When applied to the laboratory experiments of jets and forced plumes, which are axisymmetric only in the time-averaged sense, the overall results are qualitatively good and the centreline concentration and density measurements are quantitatively good. For both plumes and fountains, the relative density near the source was found to change radially as a Gaussian near the centreline. The measurements were less reliable at greater radial distances, where light attenuation tended to over-predict the relative density, where disturbances were more transient.

The quantitative agreement is somewhat surprising for this application of axisymmetric light attenuation to such transient disturbances. One reason for the good agreement is that the process of inverting the intensity signal to concentration is more sensitive to intensities measured near the centreline than those radially further away. Because the signal near the centreline is stronger and less transient, the radial structure of concentrations should remain reliable some distance from the centreline. Quantifying the radial extent of the signal's reliability is the subject of future work.

In the study of double diffusive fountains, in most experiments we found that the maximum height depended only upon the total buoyancy flux resulting from the sum of the buoyancy fluxes due to heat and salinity. This result is consistent with studies showing that the turbulent diffusivities of heat and salt are approximately equal[13] although their molecular diffusivities differ by nearly two orders of magnitude. Nonetheless, if the net buoyancy flux is nearly zero and the source momentum not too large, a fountain can warm the ambient above it resulting in mixed fountain- and plume-like behaviour.

Although the problem of H_2S dispersion from sour gas flares is much more complicated than the experiments examined here, this idealized study has shown that substance and heat should diffuse equivalently provided the flow remains turbulent. Because the burned gas emanating from the top of a flare stack is buoyant, it will remain buoyant and rise turbulently as a plume; as the effluent-air mixture cools, the concentration of H_2S in the dispersing flow should decrease in kind. If cooled H_2S is to become negatively buoyant and return to the ground, it can do so only if turbulent processes in the plume are quenched. This can occur if the plume evolves to become a fountain as it rises in a stratified atmosphere.[39,40] We have seen that buoyancy fluxes associated with heat and substance can become disproportional at a fountain top. The descending fluid from a fountain in stratified fluid may not return to the ground, but spread horizontally instead at a level of neutral buoyancy.[2] Even in this case, we expect that heat and substance diffusion should differ so that the dense component may eventually descend to the ground. These processes are being examined in ongoing research.

ACKNOWLEDGMENTS

This work was supported by funding from the Canadian Foundation for Climate and Atmospheric Sciences (CFCAS GR-614) and the Natural Sciences and Engineering Research Council's USRA program. The authors would like to thank Malte Volkwein, who assisted in the image processing of some of the experiments.

APPENDIX A: BEST-FIT GAUSSIAN PROCEDURE

From radial profiles of density $\rho(r)$, such as those shown in Figures 8 and 10, we used the data for small r to determine parameters describing the magnitude A and standard deviation σ of

the best-fit Gaussian curve $f(r) = A\exp(-r^2/2\sigma^2)$. One method to determine these parameters is by taking the logarithm of successive values of f and fitting a quadratic to the result. However, this method produces a bias to large r where f is close to zero. Because the light attenuation methods produces best results near $r = 0$, we have developed an alternate methodology, which is described here.

Only discrete data for small r_i with $|\Delta\rho(r_i)| > 0.5|\Delta\rho(0)|$ are included in the analysis. The standard deviation is found by computing $\rho'/\rho \simeq [(\rho(r_{i+1}) - \rho(r_{i-1}))/(2\Delta r)]/\rho(r_i)$ for each r_i and then finding the slope of the best-fit line through the data as a function of r_i. Because for an idealized Gaussian $f'/f = -r/\sigma^2$, the slope of f'/f vs r gives the value $-1/\sigma^2$. From this we find σ.

Given σ, the Gaussian magnitude A is determined from a least-squares fit so that

$$A = \frac{\sum \rho(r_i)\exp(-{r_i}^2/2\sigma^2)}{\sum \exp(-{r_i}^2/2\sigma^2)}.$$

APPENDIX B: COMPARING FOUNTAIN AND DIFFUSION SCALES

In the Lagrangian theory for plumes and fountains,[2,41] the radius of the fountain core is assumed to increase at a constant rate with height. For a top-hat fountain emanating from a point source at the origin, the radius is $r = \beta z$, in which β is determined empirically from experiments. By comparison with the Eulerian approach of Morton *et al.*,[4] the spreading parameter is related to the entrainment coefficient, α by $\beta = 6\alpha/5$. Different experimental approaches[3,35,41] have determined the spreading parameter to range between $\beta \simeq 0.17$ and 0.23.

For a fluid parcel leaving the source at time $t = 0$, its height after time t is[3]

$$z(t) = \frac{2}{\sqrt{3\beta\sqrt{\pi}}} H_\star \left[1 - \left(1 - \frac{F_0 t}{M_0}\right)^{3/2}\right]^{1/2},$$

in which $H_\star$ is the characteristic height scale given by (16). After time $T_0 \equiv M_0/F_0$, it reaches the maximum height

$$H_0 = (2/\sqrt{3\beta\sqrt{\pi}})\, H_\star. \tag{B1}$$

This evaluates to $2.1H_\star$, consistent with Lee and Chu[41] and Turner,[9] if we use $\beta = 0.17$.

So, the distance from the top of the fountain is given as a function of time $\tau = T_0 - t$ by

$$H_0 - z(T_0 - \tau) \simeq H_0 \left[\frac{1}{2}\left(\frac{F_0}{M_0}\tau\right)^{3/2}\right], \tag{B2}$$

in which it has been assumed $\tau/T_0 \ll 1$.

Using these results, we wish to consider diffusive processes that take place as a fluid parcel reverses propagation direction near the top of the fountain. Idealizing the fountain top as a hemispherical cap,[12] the characteristic height scale for the top of the fountain is the same as its radius at maximum height: $R_0 \equiv \beta H_0$. Using (B2), we estimate the time to traverse this distance as $\tau_0 = (2\beta)^{2/3} T_0$. The corresponding length-scale for molecular diffusion over this time is $\delta_\kappa = \sqrt{\kappa\tau_0}$, in which κ is the diffusivity. Comparing this with the height-scale of the fountain top and simplifying algebraically, we find

$$\frac{\delta_\kappa}{R_0} = \frac{\sqrt{3\sqrt{\pi}}}{2^{2/3}}\beta^{1/6}\left[\frac{\kappa^2}{M_0}\right]^{1/4} = \mathcal{C}\left[\frac{\kappa^2}{M_0}\right]^{1/4}. \tag{B3}$$

For β holding values between 0.17 and 0.23, the dimensionless coefficient $\mathcal{C} \simeq 1.1$. Because (B3) depends on the initial momentum flux, but not the buoyancy flux, we may separately consider the influence of heat and salt diffusion upon the evolution of a double-diffusive fountain.

[1] J. R. O. Beauchamp, J. S. Bus, J. A. Popp, C. J. Boreiko, and D. A. Andjelkovich, "A critical review on the literature on hydrogen sulfide toxicity," Crit. Rev. Toxicol. **13**, 25–97 (1984).

[2] J. K. Ansong, P. J. Kyba, and B. R. Sutherland, "Fountains impinging upon a density interface," J. Fluid Mech. **595**, 115–139 (2008).
[3] J. K. Ansong, A. Anderson-Frey, and B. R. Sutherland, "Turbulent fountains in one- and two-layer crossflows," J. Fluid Mech. **689**, 254–278 (2011).
[4] B. R. Morton, G. I. Taylor, and J. S. Turner, "Turbulent gravitational convection from maintained and instantaneous sources," Proc. R. Soc. London, Ser. A **234**, 1–23 (1956).
[5] B. R. Morton, "Forced plumes," J. Fluid Mech. **5**, 151–163 (1959).
[6] G. Briggs, "Plume rise," Tech. Rep. TID-25075, NTIS (USAEC Critical Review Series), 1969.
[7] D. Hoult, J. Fay, and L. Forney, "Theory of plume rise compared with field observations," J. Air Pollut. Control Assoc. **19**, 585–590 (1969).
[8] E. J. List, "Turbulent jets and plumes," Annu. Rev. Fluid Mech. **14**, 189–212 (1982).
[9] J. S. Turner, "Jets and plumes with negative or reversing buoyancy," J. Fluid Mech. **26**, 779–792 (1966).
[10] T. J. McDougall, "Negatively buoyant vertical jets," Tellus **33**, 313–320 (1981).
[11] W. Lindberg, "Experiments on negatively buoyant jets, with and without cross-flow," in *NATO Advanced Research Workshop on "Recent Advances in Jets and Plumes,"* Vol. NATO ASI Series E (Kluwer Academic, Dordrecht, The Netherlands, 1994), Vol. 255, pp. 131–145.
[12] L. J. Bloomfield and R. C. Kerr, "A theoretical model of a turbulent fountain," J. Fluid Mech. **424**, 197–216 (2000).
[13] J. S. Turner, "The influence of molecular diffusivity on turbulent entrainment across a density interface," J. Fluid Mech. **33**, 639–656 (1968).
[14] C. J. Chen and W. Rodi, *Vertical Turbulent Buoyant Jets* (Pergamon, Oxford, 1980).
[15] A. Shabbir and W. K. George, "Experiments on a round turbulent buoyant plume," J. Fluid Mech. **275**, 1–32 (1994).
[16] P. N. Papanicolaou and E. J. List, "Investigations of round vertical turbulent buoyant jets," J. Fluid Mech. **195**, 341–391 (1988).
[17] S. Funatani, N. Fujisawa, and H. Ikeda, "Simultaneous measurement of temperature and velocity using two-colour LIF combined with PIV with a colour CCD camera and its application to the turbulent buoyant plume," Meas. Sci. Technol. **15**, 983–990 (2004).
[18] S. B. Dalziel, "Rayleigh-Taylor instability: Experiments with image analysis," Dyn. Atmos. Oceans **20**, 127–153 (1993).
[19] J. M. Holford and S. B. Dalziel, "Measurements of layer depth in a two-layer flow," Appl. Sci. Res. **56**, 191–207 (1996).
[20] C. Cenedese and P. F. Linden, "Cyclone and anticyclone formation in a rotating stratified fluid over sloping bottom topography," J. Fluid Mech. **381**, 199–223 (1999).
[21] C. Cenedese and P. F. Linden, "Stability of a buoyancy-driven coastal current at a shelf break," J. Fluid Mech. **452**, 97–121 (2002).
[22] R. J. Munro and S. B. Dalziel, "Attenuation technique for measuring sediment displacement levels," Expt. Fluids **39**, 600–611 (2005).
[23] P. F. Linden and J. M. Redondo, "Molecular mixing in Rayleigh-Taylor instability. Part 1: Global mixing," Phys. Fluids A **3**, 1269–1277 (1991).
[24] P. F. Linden, J. M. Redondo, and D. L. Youngs, "Molecular mixing in Rayleigh-Taylor instability," J. Fluid Mech. **265**, 97–124 (1994).
[25] S. J. Barnett, "A vertical buoyant jet with high momentum in a long ventilated tunnel," J. Fluid Mech. **252**, 279–300 (1993).
[26] U. P. Gilmour and A. W. Woods, "Mixing experiments on fluid released near the closed end of a two-dimensional channel," J. Hazard. Mat. **36**, 227–247 (1994).
[27] J. Hacker, P. F. Linden, and S. B. Dalziel, "Mixing in lock-release gravity currents," Dyn. Atmos. Oceans **24**, 183–195 (1996).
[28] B. Shamoun, M. E. Beshbeeshy, and R. Bonazza, "Light extinction technique for void fraction measurements in bubbly flow," Expt. Fluids **26**, 16–26 (1999).
[29] D. M. Leppinen and S. B. Dalziel, "A light attenuation technique for void fraction measurement of microbubbles," Expt. Fluids **30**, 214–220 (2001).
[30] L. Hesselink, "Digital image processing in flow visualisation," Annu. Rev. Fluid Mech. **20**, 421–485 (1988).
[31] J. S. Turner, *Buoyancy Effects in Fluids* (Cambridge University Press, Cambridge, England, 1973) p. 367.
[32] N. Kaye, "Turbulent plumes in stratified environments: A review of recent work," Atmos. Oceans **46**, 433–441 (2008).
[33] H. Rouse, C.-S. Yih, and H. W. Humphreys, "Gravitational convection from a boundary source," Tellus **4**, 201–210 (1952).
[34] J. S. Turner, "Buoyant plumes and thermals," Annu. Rev. Fluid Mech. **1**, 29–44 (1969).
[35] W. Baines and V. Chu, "Jets and Plumes," in *Environmental Hydraulics* (Kluwer Academic, Dordrecht, The Netherlands, 1996), Chap. 2, pp. 7–61.
[36] J. S. Turner and H. Stommel, "A new case of convection in the presence of combined vertical salinity and temperatuer gradients," Proc. Nat. Acad. Sci. **52**, 49–53 (1964).
[37] P. F. Linden and T. G. L. Shirtcliffe, "The diffusive interface in double-diffusive convection," J. Fluid Mech. **87**, 417–432 (1978).
[38] R. Schmitt, "Double diffusion in oceanography," Annu. Rev. Fluid Mech. **26**, 255–285 (1994).
[39] L. J. Bloomfield and R. C. Kerr, "Turbulent fountains in a stratified fluid," J. Fluid Mech. **358**, 335–356 (1998).
[40] J. K. Ansong and B. R. Sutherland, "Internal gravity waves generated by convective plumes," J. Fluid Mech. **648**, 405–434 (2010).
[41] J. Lee and V. Chu, *Turbulent Buoyant Jets and Plumes: A Langrangian Approach* (Kluwer Academic, Dordrecht, The Netherlands, 2003).